

Preparation of porous LSM powders using a pore-forming agent by an ultrasonic spray pyrolysis method

Young-Hoon Choi¹, Segoo Kang¹, Jürgen Wackerl², Kyoung-Tae Lim³, Doo-Hwan Jung¹,
Taejin Kim⁴ and Dong-Hyun Peck^{1,*}

¹Korea Institute of Energy Research (KIER), 152 Gajeong, Yuseong, Daejeon 305-343, Republic of Korea

²Institute of Energy Research (IEK-3), Research Centre Jülich (FZJ), Jülich 52425, Germany

³Kceracell Co., Ltd, 533-1 Yongsan, Yuseong, Daejeon 305-501, Republic of Korea

⁴Daegyeong Institute for Regional Program Evaluation, 300 Sampung, Gyeongsan, Gyeongbuk 712-210, Republic of Korea

A novel fabrication method for porous LSM (lanthanum strontium manganite) powders using a pore-forming agent was developed by an ultrasonic spray pyrolysis (USP) method. The spray solution was prepared for the chemical composition of LSM ($(La_{0.85}Sr_{0.15})_{0.9}MnO_{3-\delta}$) by dissolving proper amounts of La-, Sr- and Mn-nitrates in distilled water. To form a porous-structured LSM powder, hollow polymer particles as a pore-forming agent were mixed with a solution of nitrates. The solution of this mixture was atomized by an ultrasonic nebulizer. The atomized droplets were decomposed and synthesized in the hot zone of a furnace at 650 °C. The morphology and crystal phases of the powders were studied by SEM, TEM and XRD. Thermal analyses of the nitrate precursors and synthesized powders were performed using DSC/TG. The particle size of the prepared powders was determined by a particle size analyzer. The structure of the porous cathode layer for a cell was fabricated by a dip-coating process using porous LSM powders. The morphology and microstructure of the coated porous cathode layer were characterized by SEM.

Key words: Lanthanum strontium manganite, Porous powder, Cathode, Pore-forming agent, Ultrasonic spray pyrolysis method.

Introduction

The overall losses in a solid-oxide fuel cell (SOFC) are controlled to a great extent by the cathodic reaction. Cathodic polarization resistance is caused by the oxygen reduction reaction (ORR) and the associated reaction and transport processes. The ORR kinetics often significantly limits the performance of a SOFC. To obtain a high level of performance from a cathode, optimizing the porous cathode layer with regard to the material and the microstructure of the cathode is necessary. Many attempts have been made to enhance the cathode performance by optimizing the material, the microstructure, and the electrolyte interface of the cathode [1-3]. The ORR in porous electrodes occurs around the triple-phase boundary (TPB) region, where the reactive gas comes in contact with the electrolyte and electrode. The reaction rate of the ORR is controlled by the interfacial reactions in the TPB region. The cathodic polarization resistance is closely related to the material and microstructure of the cathode and the TPB. Therefore, optimizing the TPB in SOFCs is very important to improving the performance

of fuel cells. Studies of the TPB are extensive in the literature on SOFCs, and much effort has been made to delineate the properties of the TPB clearly [4-6].

The properties of the cathode material require stability at 1200 K in air, high electronic conductivity, high electro-catalytic activity, and low reactivity with electrolyte materials. Perovskite metal oxides with the composition of $La_{1-x}Sr_xMnO_3$ (strontium doped lanthanum manganite, LSM) are most commonly used as cathode materials for SOFCs due to their high electro-catalytic activities, good chemical stability and electronic conductivity in oxidizing atmospheres. Strontium doping enhances the electronic conductivity of $LaMnO_3$ due to the increased the Mn^{4+} content which results from the substitution of La^{3+} by Sr^{2+} [1-3]. The performance of a LSM cathode material of SOFC is influenced by not only the chemical stability and thermodynamics characteristics of the LSM of the cathode material but also by its microstructure, grain and pore size, and pore size distribution. In particular, a porous microstructure and the pore size distribution play significant roles in terms of the permeability of oxygen gas and in reducing oxygen to oxygen ions.

Thus far, many different methods have been utilized to synthesize LSM powder, such as co-precipitation [7, 8], sucrose combustion [9] and sol-gel [10, 11] methods. However, there are only a few reports on the preparation of porous LSM powder. Recently, many

*Corresponding author:
Tel : +82-42-860-3501
Fax: +82-42-861-6224
E-mail: dhpeck@kier.re.kr

researchers have focused on the fabrication of porous ceramic materials. It has been recognized that porous ceramic materials can be fabricated using a mixture of ceramic powder and additional polymers as pore-forming agents, which burn out at low temperatures and form small and homogenous pores. Porous zirconia [12] and PZT (lead zirconate titanate) [13] ceramics were fabricated using ceramic powder and different volume percentages of polymethylmethacrylate (PMMA) powders as pore-forming agents. Porous M/Ti (M = Zr or Ta) oxides [14], Mg-Al hydroxides [15], 3Y-ZrO₂ [16], Ce_{1-x}Zr_xO₂ beads [17], TiO₂ (Titania) hollow spheres [18] and ZnO porous thin film [19] were prepared by impregnation or surface-coating processes using a polystyrene (PS) sphere as a template. PS spheres were chosen because they can be easily removed by dissolution or after slight calcination. However, while these methods have been applied for the production of porous ceramic bodies or coated hollow spheres, they are limited when used for the synthesis of porous ceramic powders.

Ultrasonic spray pyrolysis (USP) is thought to be an effective technique for an inexpensive and continuous ambient-pressure process of creating non-agglomerated powders with homogeneous compositions. This process is considered to be a method which can produce multicomponent powders and films such as ZrO₂ and CeO₂ [20], PZT [21], LSM-YSZ [22], Li_MMn_{2-x}O₄ (M=Al, Cr, Fe and Co) [23], metal Co powder [24], YSZ [25], nano-sized MgO [26], nano-sized Y₂O₃ [27], nano-sized BaTiO₃ [28]. These methods have been used to prepare ultrafine spherical powders. Skrabalak and Suslick [29] applied the USP method to prepare porous MoS₂. However, in their study the prepared SiO₂/MoS₂ composite required a special treatment with HF to remove the silica used as a sacrificial template and leave the porous MoS₂. Suh and Suslick [30] used the USP process to prepare a cobalt-doped porous silica nano-sphere from a silica/organic polymer (ethylene glycol) composite, followed by a second heating to pyrolyze and remove the polymer. This process has some disadvantages in that the morphology of the final porous sphere is very sensitive when varying the silica-polymer ratio. Moreover, the pore size is not homogeneous.

The USP method was employed in this work to synthesize porous-structured LSM powders with the composition of (La_{0.85}Sr_{0.15})_{0.9}MnO_{3-δ}. In order to increase the porosity of the LSM powders, hollow polymer particles as a pore-forming agent were added to the mixture of a metal nitrate solution and water. The powder was characterized for its microstructure and pore size distribution. The structure of the porous cathode layer for a cell was fabricated by a dip-coating process using the porous LSM powders. The morphology and microstructure of the coated porous cathode layer were characterized.

Experimental

The LSM ((La_{0.85}Sr_{0.15})_{0.9}MnO_{3-δ}) powder was prepared by the USP method. The metal nitrates La(NO₃)₃ · 6H₂O (Sigma-Aldrich Co.), Sr(NO₃)₂ (Sigma-Aldrich Co.), and Mn(NO₃)₂ · 4H₂O (Sigma-Aldrich Co.) were used as starting raw materials. The nitrate solution was prepared from a stoichiometric mixture of nitrate in distilled water for the USP method. The concentration of nitrates was fixed at 0.1 mol/l. LSM powders was prepared by the USP method using nitrate solutions (denoted as *LSM-N*). To form a porous-structured LSM powder, the hollow polymer particles (polystyrene (PS) sphere) as a pore-forming agent were mixed with the solution of nitrates (denoted as *LSM-NP*). The concentration of the hollow polymer particles in the nitrate solution ranged from 0.5 to 4 wt%. The mean particle diameter (*d*₅₀) of the hollow polymer particle was about 0.5 μm. They had a very homogenous size distribution and were smooth and perfectly spherical. The solution containing this mixture was atomized by an ultrasonic nebulizer with a resonant frequency of 1.7 MHz. A carrier gas (air) was used to carry the sprayed droplets through a quartz tube (50 mm in diameter) at a flow rate of 20 l/min. Droplets of the solution were decomposed in the hot zone of a furnace at 650 °C. The prepared particles were annealed at 650 °C to crystallize the powders and to decompose the residual organic content. To compare the microstructures of the coated LSM layers depending on the LSM powder type and the sintering temperature, LSM powder was also prepared by a solid-state reaction (at 1000 °C for 5 h.) using a mixture of La₂O₃, SrCO₃, and MnO₂ as the starting materials (denoted as *LSM-S*).

The morphology of the synthesized LSM powder was investigated using a scanning electron microscope (FE-SEM, S-4700, Hitachi) equipped with an energy dispersive X-ray analyzer (EDX) and a transmission electron microscope (FE-TEM, Carl Zeiss, EMP12 Omega). The particle size distribution and pore size of the synthesized LSM powder were investigated by means of electrophoretic light scattering (ELS-8000, Otsuka Electronics) and BET (Tristar 3000, Micromeritics). The crystal phases of the synthesized powders were confirmed by powder X-ray diffractometry (XRD, Rigaku). In addition, the thermal decomposition properties of the mixture of the nitrates and hollow polymer particles were investigated using a DSC/TGA (STA 409PC, Netzsch).

Ni/YSZ cermet, ScMnSZ [(ZrO₂)_{0.89}(Sc₂O₃)_{0.1}(MnO₂)_{0.01}], and LSM [(La_{0.85}Sr_{0.15})_{0.9}MnO_{3-δ}] powder were used as the materials for anode-supported tube, the electrolyte, and the cathode, respectively. The ScMnSZ powder used as a dense electrolyte layer was prepared by the Pechini method. The extruded anode-supported tube serves as the fuel electrode, and the other cell components were coated in the form of thin layers onto

it. The ScMnSZ electrolyte layer was coated on the pre-sintered anode tube by a slurry dip-coating process to form a dense layer. It was sintered at 1400 °C. The porous LSM cathode layers was also coated by a dip-coating process on a dense electrolyte layer and sintered at 1200 °C. The electrode area of the anode-supported tubular single cell was 9.4 cm². The length and circumference of the electrode were 5 cm and 1.8 cm, respectively. The microstructure of the porous cathode layer for a single cell was investigated by means of SEM.

Result and Discussion

Fig. 1 shows a SEM micrograph of the hollow polymer particles (polystyrene (PS) sphere) used as pore-forming agent. The hollow polymer particles were extremely uniform with a mean particle diameter (d_{50}) of 0.5 μm [15-16]. They had a very homogenous size distribution and were smooth and perfectly spherical, as shown in Fig. 1. To prepare a porous-structured LSM powder by the USP method, the hollow polymer particle as a pore-forming agent were mixed with a solution of nitrates for the composition of LSM ((La_{0.85}Sr_{0.15})_{0.9}MnO_{3- δ}). The concentration of the hollow polymer particles in the nitrate solution ranged from 0.5 to 4 wt%.

The curves of the simultaneous DSC and TGA behavior of the mixture of the nitrates and the hollow

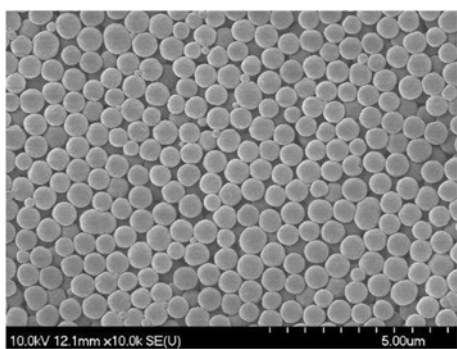


Fig. 1. SEM image of the hollow polymer particles used as a pore-forming agent.

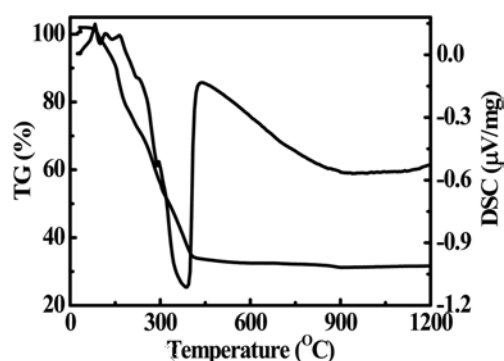


Fig. 2. DSC/TG curve of the mixture of metal nitrates and hollow polymer particles.

polymer particles used as a pore-forming agent are shown in Fig. 2. The endothermic peak below 150 °C may be due to the loss of adsorbed water, while the exothermic peak in the temperature range of 150–200 °C can be attributed to the partial decomposition of the nitrates and the charring of the hollow polymer particles. The endothermic peak between 200 °C and 400 °C corresponds to the complete dissociation of the nitrates and the polymer and initiation of the formation of the LSM phase. This result shows that the hollow polymer particles can be used as a pore-forming agent for the preparation of porous LSM powder by the USP method.

SEM micrographs of the *LSM-N*, which was calcined at 650 °C for 5 h are shown in Fig. 3. Fig. 3(a) shows a SEM photograph of typically synthesized *LSM-N*, where small particles between 0.05 and 0.1 μm in size constitute one large spherical particle (0.1–1 μm) of LSM powder. The primary particles appeared as single spherical crystals with a nearly uniform size. Moreover, the directional linkage of the particles was observed. Fig. 3(b) shows a SEM photograph of a hollow particle with an open shape. This type of particle was not found often. This result shows that the *LSM-N* consists of a hollow sphere and that the hollow spheres consist of small particles.

Typical SEM micrograph of the porous *LSM-NP*, which was calcined at 650 °C for 5 h presented in Fig. 4(a). Fig. 4(b) is an enlarged image of the porous regions shown in Fig. 4(a). A cluster of small particles on the surface of the synthesized spherical powders was observed, as shown in Fig. 4(b). The clusters of small particles resemble sea anemones with isolated regions. These clusters are 0.3–0.5 μm in size, as

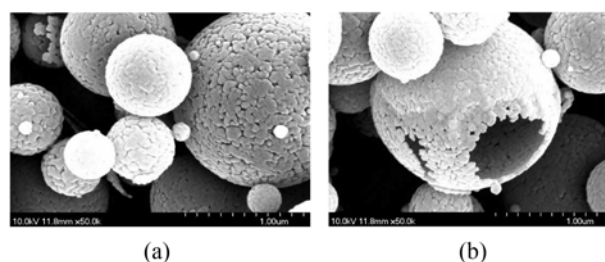


Fig. 3. SEM images of the *LSM-N* (a: closed hollow spheres, b: open hollow spheres) (calcined at 650 °C).

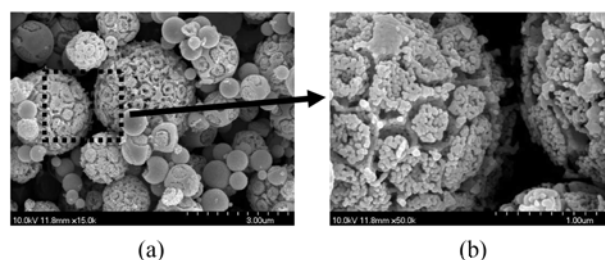


Fig. 4. SEM images of the *LSM-NP* (a), and an enlarged image of the porous regions (b) (calcined at 650 °C).

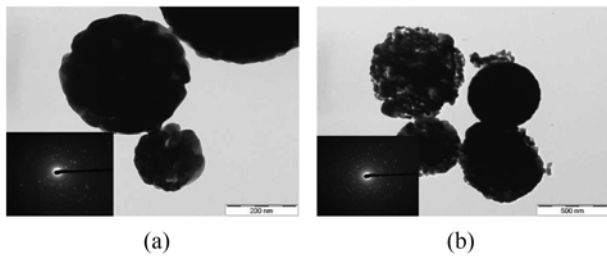


Fig. 5. TEM images and ED patterns (inset) of the *LSM-N* (a) and the *LSM-NP* (b) samples.

shown in Fig. 4(b). This size is similar to that of the hollow polymer particles used a pore-forming agent ($d_{50} = 0.5 \mu\text{m}$). This may indicate that the formation of this cluster is related to the properties and states of the hollow polymer particles. The morphology of the powder can be attributed to the solubility of the nitrates and the viscosity of the sprayed solution [20]. In our earlier studies of USP methods using ZrO_2 -based materials, the morphologies of the synthesized powders were found to vary significantly with the concentration and the viscosity of the sprayed solutions [21].

TEM images and the electron diffraction (ED) patterns of the *LSM-N* (a), and the *LSM-NP*(b) are presented in Fig. 5. The TEM images in Figs. 5(a) and (b) indicate that the powders are hollow, showing clusters of particles. The ED patterns indicate that the compositions exhibit polycrystalline structures.

Fig. 6 shows SEM images of *LSM-NP* with different powder shapes as synthesized by the USP method at 650°C using a mixture of the nitrate solution and hollow polymer particles. The cluster of small particles on the surface of the synthesized spherical powders shows slightly different shapes. However, the size of this cluster was mainly in the range of $0.3 - 0.5 \mu\text{m}$, as shown in Fig. 6. The size is also similar to that of the hollow polymer particles used as a pore-forming agent ($d_{50} = 0.5 \mu\text{m}$). The morphology of the powder can be attributed to the solubility of the nitrates and the viscosity of the sprayed solution [20].

The XRD patterns of the as-synthesized LSM powder samples, and the samples calcined at different temperatures ($650^\circ\text{C} - 1200^\circ\text{C}$) for 5 h are exhibited in Fig. 7. The as-synthesized *LSM-N* (Fig. 7(a)) and *LSM-NP* (Fig. 7(b)) were prepared by the USP method at 650°C . The as-synthesized *LSM-N* and *LSM-NP* show a non-crystalline phase, which was not identified in the

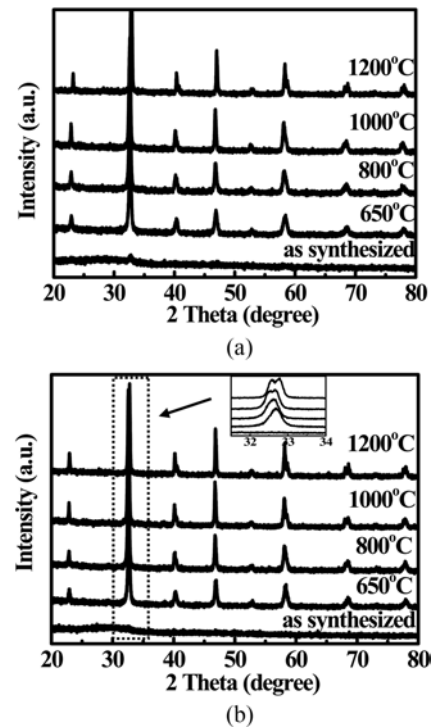


Fig. 7. XRD patterns of the as-synthesized LSM powder, and calcined *LSM-N* (a) and *LSM-NP* (b) samples at different temperatures ($650^\circ\text{C} - 1200^\circ\text{C}$) for 5 h.

XRD results. Calcination of the as-synthesized powder in air above 650°C for 5 h significantly changed the XRD patterns [22]. A single LSM perovskite phase was obtained for all the samples calcined in air above 650°C for 5 h, as shown in Figs. 7(a) and 7(b). Enlarged XRD patterns in the range $2\theta = 31.5 \sim 34^\circ$ are shown in Fig. 7(b). The crystal phases of the calcined samples at temperatures of 650°C and 800°C showed an orthorhombic structure, whereas when the samples were calcined at 1000°C and 1200°C , the structure of the material was transformed into a rhombohedral structure, as shown in Fig. 7(b). This type of phase transformation of the crystal structure was also observed in the samples shown in Fig. 7(a).

Fig. 8 shows the N_2 adsorption-desorption isotherms (a) and the corresponding BJH (Barrett-Joyner-Halenda) pore diameter curves (b) of the *LSM-S*, *LSM-N*, and *LSM-NP*, respectively. An abrupt increase in the adsorption volume of adsorbed N_2 was observed and was associated with a P/P_0 value greater than 0.85 (by

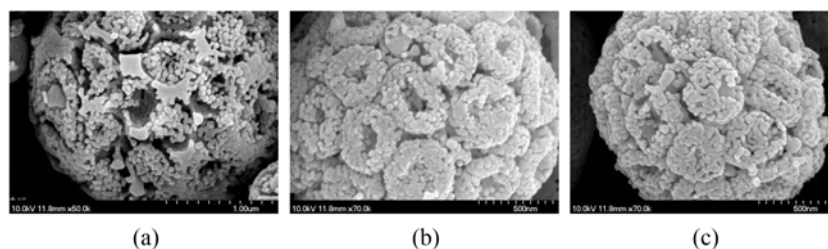


Fig. 6. SEM images of the *LSM-NP* with different shapes of powders synthesized by the same process shown in Fig. 4.

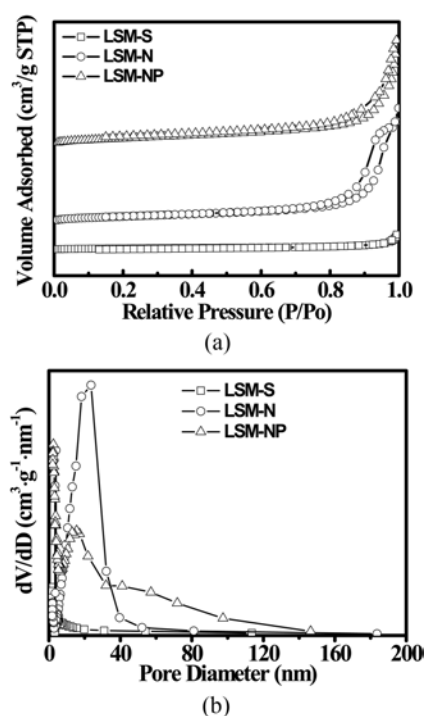


Fig. 8. N_2 adsorption-desorption isotherm (a) and pore diameters (b) of the *LSM-S*, *LSM-N*, and *LSM-NP* powders.

Table 1. Mean particle diameter, BET surface area, mean pore diameter and mean pore volume of the *LSM-S*, *LSM-N*, and *LSM-NP* powders.

Samples	Mean particle diameter (nm)	BET (m^2/g)	Mean pore diameter (nm)	Mean pore volume (cm^3/g)
<i>LSM-S</i>	274	2.72	15.38	0.0094
<i>LSM-N</i>	534	12	20.54	0.0713
<i>LSM-NP</i>	346	14.73	17.27	0.0658

the USP method). This sharp increase is generally associated with the capillary condensation of nitrogen in pores. In the porous structures of the *LSM-NP*, the absorption/desorption isotherm curve is more reversible than that of the *LSM-N*. This result indicates that the porous structure of the *LSM-NP* has fewer closed pores and no obvious pore-blocking effects [14, 18].

The mean particle diameter, BET surface area, mean pore diameter and mean pore volume of the *LSM-S*, *LSM-N*, and *LSM-NP* powders obtained via the BJH method by calculating the desorption branch of the nitrogen isotherm are shown in Table 1. The mean particle diameter, BET surface area, mean pore diameter and mean pore volume of the *LSM-S*, *LSM-N*, and *LSM-NP* powders were determined to be 15.38, 20.54, and 17.27 nm, respectively (Fig. 8(b)). The corresponding BJH desorption cumulative pore volumes of the *LSM-S*, *LSM-N*, and *LSM-NP* powders are 0.0094, 0.0713, and 0.0658 cm^3/g , respectively. The measured BET surface areas of the *LSM-S*, *LSM-N*, and *LSM-NP* powders are 2.72, 12.0 and 14.73 m^2/g , respectively. The cumulative pore volumes and BET

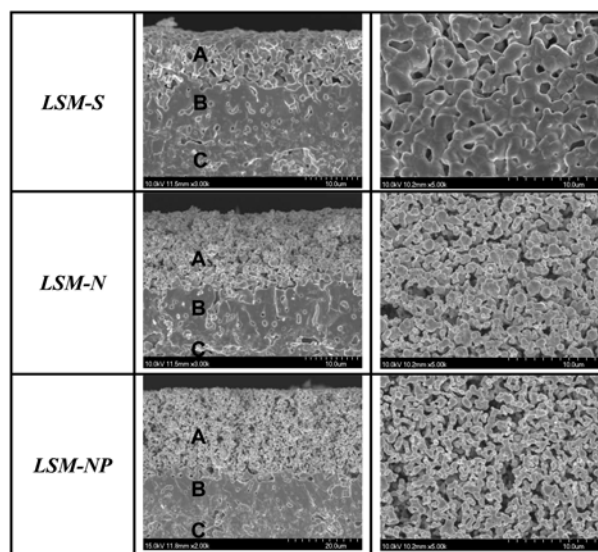


Fig. 9. SEM images of the cross-section and surface of a single cell composed of various cathode layers using the *LSM-S*, *LSM-N*, and *LSM-NP* powders (A: cathode (LSM), B: electrolyte (ScMnSZ) and C: anode (Ni/YSZ cermet)).

surface areas of the powders synthesized by the USP method (*LSM-N* and *LSM-NP*) are much higher than that of by the solid-state reaction method (*LSM-S*). The pore diameter of *LSM-NP* exists in almost every region (2–140 nm), but the pore diameter of the *LSM-N* only exists in one region (2–40 nm) due to the single hysteresis loop.

SEM images of the fractured cross-section and surface of a cell composed of various cathode layers using the *LSM-S*, *LSM-N*, and *LSM-NP* powders are shown in Fig. 9. The extruded anode-supported tube composed of Ni/YSZ cermet serves as the anode (C), and the other cell components (electrolyte (B) and cathode (A)) were coated by a slurry dip-coating process in the form of the thin layers on the pre-sintered anode tube. The porous LSM cathode layer (A) was also coated by the dip-coating process on a dense ScMnSZ electrolyte layer (B), after which it was sintered at 1200 °C. The LSM layer sintered at 1200 °C exhibits a porous microstructure. The porous LSM layer adhered well to the electrolyte layer, showing a high surface area, as shown in Fig. 9. The cathode layer prepared from the *LSM-S* powder has a relatively low porosity and larger grains, whereas the samples with the *LSM-N* and *LSM-NP* powders have higher porosities and smaller grains. The cathode layer prepared from the *LSM-NP* powder shows relatively fine pores and smaller grains compared to that prepared from the *LSM-N* powder. The microstructures of the LSM layer are affected by both the powder type and the sintering temperature [11]. The cathode layer sintered at 1000 °C and 1100 °C using the *LSM-N* and *LSM-NP* powders also showed high porosities and small grains than that sintered at 1200 °C. However,

those coated LSM layers did not adhere well to the electrolyte layer and show poor connections between their cathode particles.

Conclusions

LSM powder was prepared by the USP method using a nitrate solution (*LSM-N*). To compare the microstructures of the coated LSM layers depending on the LSM powder type and the sintering temperature, the LSM powder was also prepared by a solid-state reaction method (*LSM-S*). To form a porous-structured LSM powder using the USP method, hollow polymer particles (PS) of 3 wt% as a pore-forming agent were mixed with the nitrate solution (*LSM-NP*). The primary particles resembled single spherical crystals of a nearly uniform size, showing directional linkages of the particle. A cluster of small particles on the surface of the synthesized spherical powders (*LSM-NP*) was also observed. The clusters of small particles resembled sea anemones with isolated regions. In the porous structures of the *LSM-NP*, the absorption/desorption isotherm curve is more reversible than that of the *LSM-N*. This result indicates that the porous structures of the *LSM-NP* have fewer closed pores and no obvious pore-blocking effects. The cumulative pore volumes and BET surface areas of a powder synthesized by the USP method are much higher than those of *LSM-S*. The LSM layer sintered at 1200 °C exhibits a typical porous microstructure. The porous LSM layer adhered well to the electrolyte layer showing a high surface area. The sample with *LSM-S* has a relatively low porosity, whereas the samples with *LSM-N*, and *LSM-NP* have higher porosities. The cathode layer prepared from the *LSM-NP* powder shows relatively fine pores and smaller grains compared to the pores and grains of the *LSM-N*.

Acknowledgments

This work was supported by the Joint Research Project under the Korea Research Council for Industrial Science & Technology (ISTK) and for Fundamental Science & Technology (KRCF), Republic of Korea.

References

1. W. Vielstich, A. Lamm, and H.A. Gasteiger, in "Handbook of fuel cells, Fundamentals technology and applications, V.2 Electrocatalysis" (John Wiley & Sons, 2003) pp. 587-600.
2. N.Q. Minh, *J. Am. Ceram. Soc.* 76 (1993) 563-588.
3. S.C. Singhal and K. Kendall, in "High temperature solid oxide fuel cells" (Elsevier, 2003) pp. 119-147.
4. J. Mizusaki, H. Tagawa, K. Tsuneyoshi, and A. Sawata, *J. Electrochem. Soc.* 138 (1991) 1867.
5. A. Bieberle, L.P. Meier, and L.J. Gauckler, *J. Electrochem. Soc.* 148 (2001) A646.
6. J. Fleig, *J. Power Sources*, 125 (2002) 228.
7. V. Uskokovic and M. Drogenik, *Materials and Design* 28 (2007) 667-672.
8. A. Ghosh, A.K. Sahu, A.K. Gulnar, and A.K. Suri, *Scripta Materialia* 52 (2005) 1305-1309.
9. K. Prahakaran, J. Joseph, N.M. Gokhale, S.C. Shorma, and R. Lal, *Ceramic International* 31 (2005) 327-331.
10. G. Venkataiah, V. Prasad and P.V. Reddy, *J. Alloys and Compounds* 429 (2007) 1-9.
11. R. Chiba, F. Yoshimura, Y. Sakurai, Y. Tabata, and M. Arakawa, *Solid State Ionics* 175 (2004) 23-27.
12. A.K. Gain, H.Y. Song, and B.T. Lee, *Scripta Materialia* 54 (2006) 2081-2085.
13. H.L. Zhang, J.F. Li and B.P. Zhang, *Acta Materialia* 55 (2007) 171-181.
14. C. Wang, A. Geng, S. Jiang, X. Qu, and L. Li, *J. Colloid and Interface Science* 301 (2006) 236-247.
15. E. Geraud, V. Prevot, and F. Leroux, *J. Physics and Chemistry of Solids* 67 (2006) 903-908.
16. S. Liya, L. Mingjian, and Liu Xiaozhen, *Materials Research Bulletin* 41 (2006) 1891-1901.
17. A.S. Deshpande and M. Niederberger, *Microporous and Mesoporous Materials* 101 (2007) 413-418.
18. A. Syoufian, Y. Inoue, M. Yada, and K. Nakashima, *Materials Letters* 61 (2007) 1572-1575.
19. Z. Liu, Z. Jin, W. Li, J. Qiu, J. Zhao, and X. Liu, *Applied Surface Science* 252 (2006) 5002-5009.
20. C.Y. Chen, T.K. Tseng, S.C. Tsai, C.K. Lin, and H.M. Lin, *Ceramics International* 34 (2008) 409-416.
21. Y.H. Choi, D.H. Peck, Y.C. Park, K.T. Lim, D.S. Suhr, J. Wackerl, and T. Markus, *J. Korean Ceramic Soc.* 44 (2007) 690-695.
22. S. Lee and B. Jun, *Ceramics international* 31 (2005) 53-56.
23. Z.V. Marinkovic, L. Mancic, J.-F. Cribier, S. Ohara, T. Fukui, and O. Milosevic, *Materials Science and Engineering A* 375-377 (2004) 615-619.
24. I. Taniguchi, *Materials Chemistry and Physics* 92 (2005) 172-179.
25. S. Guermen, S. Sropic, and B. Friedrich, *Materials Research Bulletin* 41 (2006) 1882-1890.
26. S. Uhlenbruck, T. Hoppe, H.P. Buchkremer, and D. Stoeber, *J. Ceramic Processing Research* 7 (2006) 214-220.
27. J.M. Han, D.S. Jung, S.H. Lee, and Y.C. Kang, *J. Ceramic Processing Research* 9 (2008) 140-145.
28. H.Y. Koo, S.H. Lee, D.R. Ko, and Y.C. Kang, *J. Ceramic Processing Research* 11 (2010) 656-659.
29. D.S. Jung, S.H. Lee, and Y.C. Kang, *J. Ceramic Processing Research* 9 (2008) 307-310.
30. S.E. Skrabalak and K.S. Suslick, *J. Am. Chem. Soc.* 127 (2005) 9990-9991.
31. W.H. Suh and K.S. Suslick, *J. Am. Chem. Soc.* 127 (2005) 12007-12010.